2013 American Control Conference (ACC)
Washington, DC, USA, June 17-19, 2013

Aliasing Effects in Direct Digital Adaptive Control of Plants with High-Frequency Dynamics and Disturbances

E. Dogan Sumer, and Dennis S. Bernstein

Abstract— **In this paper we consider sampled-data adaptive control in the presence of aliasing, due to either the high-frequency free response of the plant, or the high-frequency content in the disturbances. In particular, we present a numerical investigation of retrospective cost adaptive control (RCAC) applied to sampled-data command-following and disturbance-rejection problems, and investigate the performance of RCAC in the presence of aliasing. It is shown that RCAC is able to stabilize the plant despite the high-frequency dynamics, unless the controllability of unstable modes is not lost due to sampling. However, the intersample command-following performance may be nonzero due to aliasing of disturbances.**

I. INTRODUCTION

Because of the ability to implement nonlinear and logical operators in embedded code, as well as the ability to easily modify that code, the vast majority of modern control systems are implemented digitally. Digital controllers possess one drawback relative to analog controllers, however, namely, aliasing effects, which arise when the sampled signal possesses frequency content above the Nyquist frequency, which is half of the sampling frequency. Aliasing implies that frequency content above the Nyquist frequency is "folded" down to a lower frequency by mirror imaging its spectral content about the Nyquist frequency. The aliased harmonics of the folded signal thus constitute harmonics that are not present in the original, analog signal. Consequently, the controller may be forced to operate on an error signal that is not a true representation of the error signal that it was designed to operate on. There are two strategies for addressing the effects of aliasing. First, the sampling rate can be chosen to be significantly above the highest frequency content of the sampled signal, including both the dynamic response of the system and exogenous signals. This approach may require a sampling rate that is far beyond the required bandwidth of the system, thus entailing an undue burden on the digital hardware. For example, if the goal is to control rigid body motion but the system has a high-frequency flexible mode, then a fast sampling rate is needed in order to avoid aliasing the contribution of the flexible mode. Thus, the flexible mode may be inadvertently excited by the feedback controller.

The second approach to addressing the effects of aliasing is to employ an anti-aliasing filter. An anti-aliasing filter is a filter that is designed to roll off at a chosen frequency and thus to attenuate the frequency content of the signal above the Nyquist frequency. Anti-aliasing filters are almost always analog; a digital filter cannot reliably remove the effects of aliasing once the signal has been sampled, except perhaps as a notch filter when the aliased frequencies are known. Consequently, the analog anti-aliasing filter is a fixed component that must be engineered into the system along with the choice of sampling rate and controller bandwidth.

In summary, aliasing can be addressed by either fast sampling or analog anti-aliasing. Both approaches have drawbacks and both may be imperfect. For virtually all digital control systems, the question thus remains as to whether the effects of aliasing can degrade the performance of the closed-loop system. The goal of this paper is thus to investigate the effects of aliasing without assuming the benefits of either sufficiently fast sampling or sufficiently effective analog anti-aliasing filters.

Control under arbitrarily slow sampling is considered in [1], where it is shown that, under perfect modeling, the effects of aliasing can be addressed by sampled-data LQG control, except at sampling rates at which controllability is lost [2]. The present paper, however, focuses on the more realistic case of model uncertainty, especially at high frequencies. Within the context of adaptive control, unmodeled high-frequency dynamics are known to present difficulties, as demonstrated by the celebrated Rohrs counterexample [4]. Recently, this issue was revisited in [5] within the context of sampled-data adaptive control. Specifically, retrospective cost adaptive control (RCAC) was applied to this problem in order to determine its ability to address the effects of unmodeled high-frequency dynamics. As shown in [5], RCAC was able to follow the command despite the unmodeled modes, the unknown sinusoidal disturbance, and the unknown nonminimum-phase sampling zero contributed by the unmodeled high-frequency dynamics.

The results of [5], however, assumed that the sampling rate was sufficiently high as to avoid aliasing. The goal of the present paper is to consider adaptive control in the presence of aliasing, due to either the high-frequency free response of the plant or the high-frequency content in the disturbances. We are especially interested in the intersample behavior of the plant and performance variables as a consequence of sampling and aliasing. Within the context of fixed-gain control, intersample behavior is examined in [3, 6, 7].

II. PROBLEM FORMULATION

Consider the MIMO plant

$$\dot{\bar{x}}(t) = \bar{A}\bar{x}(t) + \bar{B}\bar{u}(t) + \bar{D}_1\bar{w}(t), \tag{1}$$

$$\bar{z}(t) = E_1\bar{x}(t) - \bar{r}(t), \tag{2}$$

The authors are with the Department of Aerospace Engineering, The University of Michigan, Ann Arbor, MI 48109-2140.

978-1-4799-0176-0/$31.00 ©2013 AACC

where $(\bar{A}, \bar{B}, \bar{E}_1)$ is minimal, $\bar{x}(t) \in \mathbb{R}^n$ is the state variable, $\bar{z}(t) \in \mathbb{R}^{l_z}$ is the performance output, $\bar{u}(t) \in \mathbb{R}^{l_u}$ is the control input, $\bar{w}(t) \in \mathbb{R}^{l_w}$ is the disturbance signal, $\bar{r}(t) \in \mathbb{R}^{l_r}$ is the reference command, and $t \geq 0$. In this paper, we assume that $w(t)$ and $r(t)$ are harmonic signals with bandwidth $\omega_{\mathrm{B},w}$ and $\omega_{\mathrm{B},r}$ respectively. Furthermore, we define $\omega_{\mathrm{N},w} = 2\omega_{\mathrm{B},w}$ and $\omega_{\mathrm{N},r} = 2\omega_{\mathrm{B},r}$ as the Nyquist rate corresponding to w and r respectively. The plant (1), (2) can be discretized for sampled-data control using sample and hold operators, as illustrated for the SISO case in Figure 1. For a zero-order-hold operator and a sampler with sampling period h sec/sample and sampling rate $\omega_{\mathrm{s}} = 2\pi/h$ rad/sample, the sampled-data system is described by

$$x(k+1) = Ax(k) + Bu(k) + f(w,k,h), \tag{3}$$

$$z(k) = E_1 x(k) - r(k), \tag{4}$$

where

$$A = e^{\bar{A}h}, \quad B = \int_{kh}^{(k+1)h} e^{\bar{A}((k+1)h-\tau)} d\tau \bar{B}, \tag{5}$$

$f(w,k,h) = \int_{kh}^{(k+1)h} e^{\bar{A}((k+1)h-\tau)} \bar{D}_1 \bar{w}(\tau) d\tau$, and $x(k)$, $u(k)$, $r(k)$ and $z(k)$ represent $\bar{x}(kh)$, $\bar{u}(kh)$, $\bar{r}(kh)$ and $\bar{z}(kh)$, respectively.

For the sampled-data system (3), a sufficient condition for controllability is given by the following proposition [2].

Proposition 2.1: A sufficient condition for complete controllability of (A, B) is to have

$$\mathrm{Im}\{\lambda_i(\bar{A}) - \lambda_j(\bar{A})\} \neq 2\pi l/h, \tag{6}$$

for all eigenvalues $\lambda_i(\bar{A})$, $\lambda_j(\bar{A})$ of $\bar{A}$ such that

$$\mathrm{Re}\{\lambda_i(\bar{A}) - \lambda_j(\bar{A})\} = 0, \tag{7}$$

for all nonzero integers l. Furthermore, condition (6), (7) is necessary as well if $l_u = 1$. ■

A weaker condition suffices for (A, E_1) to be observable [8]. Thus, (A, B, E_1) is minimal if (6), (7) is satisfied.

The input-output relationship from u to z is described by the operator matrix

$$G_{zu}(\mathbf{q}) \triangleq E_1(\mathbf{q}I - A)^{-1}B, \tag{8}$$

where $\mathbf{q}$ is the forward shift operator. Unlike the z-transform, (8) accounts for possibly nonzero initial conditions. Furthermore, for each positive integer i, $H_i \triangleq E_1 A^{i-1} B$ is the i^{th} Markov parameter of G_{zu}.

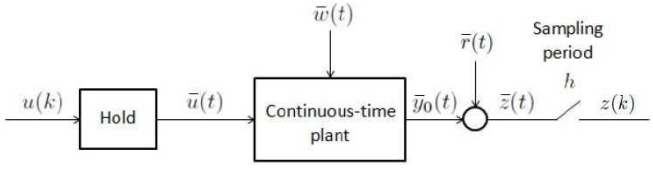

Fig. 1. Typical sampled-data system.

Now, consider the $n_{\mathrm{c}}^{\mathrm{th}}$-order strictly proper output feedback controller

$$x_{\mathrm{c}}(k+1) = A_{\mathrm{c}}(k)x_{\mathrm{c}}(k) + B_{\mathrm{c}}(k)z(k), \tag{9}$$

$$u(k) = C_{\mathrm{c}}(k)x_{\mathrm{c}}(k), \tag{10}$$

where $x_{\mathrm{c}} \in \mathbb{R}^{n_{\mathrm{c}}}$. The feedback control (9), (10) is represented by $u = G_{\mathrm{c}}(\mathbf{q}, k)z$, where

$$G_{\mathrm{c}}(\mathbf{q}, k) \triangleq C_{\mathrm{c}}(k)(\mathbf{q}I - A_{\mathrm{c}}(k))^{-1}B_{\mathrm{c}}(k). \tag{11}$$

The closed-loop system with output feedback (9), (10) is thus given by

$$\tilde{x}(k+1) = \tilde{A}\tilde{x}(k) + \tilde{f}(w,k,h), \tag{12}$$

$$z(k) = \tilde{E}_1 \tilde{x}(k) + E_0 r(k), \tag{13}$$

where

$$\tilde{A} \triangleq \begin{bmatrix} A & BC_{\mathrm{c}} \\ B_{\mathrm{c}}E_1 & A_{\mathrm{c}} \end{bmatrix}, \quad \tilde{f}(w,k,h) \triangleq \begin{bmatrix} f(w,k,h) \\ 0 \end{bmatrix},$$

$$\tilde{E}_1 \triangleq \begin{bmatrix} E_1 & 0_{l_z \times n_{\mathrm{c}}} \end{bmatrix}, \tag{14}$$

and $\tilde{x}(k) = \begin{bmatrix} x^{\mathrm{T}}(k) & x_{\mathrm{c}}^{\mathrm{T}}(k) \end{bmatrix}^{\mathrm{T}} \in \mathbb{R}^{n+n_{\mathrm{c}}}$.

From a sampled-data point of view, the objective is to develop an adaptive output feedback controller to minimize $z^{\mathrm{T}}(k)z(k)$ in the presence of the disturbance signal $\bar{w}(t)$ and the reference command $\bar{r}(t)$ with limited modeling information about the dynamics, disturbance signal, and command signal. We assume that the measurement of the performance variable $z(k)$ is available for feedback. However, having $z(k)$ near zero at every sample k does not guarantee that $\bar{z}(t)$ is small for all t. Therefore, in practice, the objective is to design a sampled-data adaptive controller to minimize $\bar{z}(t)$ not only at the sampling instants $t = kh$, but for all t.

In practice, the effects of aliasing may be mitigated by filtering the performance output $\bar{z}(t)$ with an anti-aliasing filter to decrease the bandwidth of the cascade continuous-time plant. Indeed, this would facilitate the problem for the adaptive controller since the high-frequency components due to $\bar{w}(t)$ and internal dynamics would be filtered out from the performance measurement. But this would go against the goal of this paper, which is to study the effects of aliasing in digital adaptive control. Thus, we apply adaptive control using the sampled measurements of $z(k)$ directly, with no intermediate anti-aliasing filters acting on $\bar{z}(t)$.

III. Retrospective Cost Adaptive Control

Retrospective cost adaptive control (RCAC) is a direct, discrete-time adaptive control technique that is applicable to stabilization, command following and disturbance rejection in sampled-data LTI systems [9, 10]. RCAC requires knowledge of the first nonzero Markov parameter, and the nonminimum-phase (NMP) zeros of the open-loop plant; otherwise, RCAC requires no matching assumptions on the command or the disturbance, and no information about the command or disturbance spectra are required. This modeling information is used in the construction of a finite-impulse-response filter $G_{\mathrm{f}}(\mathbf{q}^{-1})$ which is employed in controller update law. RCAC update law is based on the optimization of a cumulative cost function. The key tuning components of RCAC involve the initial RLS covariance matrix P_0 which affects the convergence speed of the algorithm, and the controller order n_{c}, which is required to be sufficiently large for internal model control. It is shown in [10] for

SISO plants that, if $G_{\rm f}(\mathbf{q}^{-1})$ captures the NMP zeros and the first nonzero Markov parameter of the open-loop plant, then the control input u is bounded, and the performance variable z asymptotically converges to zero. Extensions of this algorithm are presented in [5, 11–13] which alleviate the need to know the NMP zeros of the open-loop plant by extending the cost function with a performance-dependent control penalty.

IV. Numerical Examples with Disturbance Aliasing

We now investigate the performance of RCAC with undersampling of disturbances, that is, the continuous-time plant is sampled at a rate slower than the Nyquist rate corresponding to the disturbance $\bar{w}(t)$ so that $\omega_{\rm s} < \omega_{{\rm N},w}$. In each example, the controller $\Theta(k)$ is initialized to be zero, and cumulative RCAC is used with $\lambda = 1$ to update the controller.

Example 4.1: [Undersampled disturbances.] Consider the third-order continuous-time plant $T_{zu}(s) = T_0(s)\Lambda(s)$ with $T_0(s) = \frac{2}{s+1}$ and $\Lambda(s) = \frac{229}{(s-15-\jmath 2)(s-15+\jmath 2)}$. This plant is used in [4] to show that if the fast poles contributing by $\Lambda(s)$ are ignored, traditional continuous-time MRAC may lead to an unstable closed-loop system. Sampled-data adaptive control of Rohrs counterexamples with RCAC is extensively covered in [5], where it is shown that the pulse transfer function $G_{zu}(z)$ corresponding to $T_{zu}(s)$ has a NMP sampling zero for sampling frequencies larger than 10π rad/sample. In this example, we consider a problem where the sampling rate is chosen so that the sampled-data plant is minimum-phase. Furthermore, the control objective is to follow the reference command $\bar{r}(t) = 2 + \sin t$, and the only modeling information available is the first Markov parameter H_1 of G_{zu}.

First, we consider the case with no disturbances. Choosing $n_{\rm c} = 10$ and $P_0 = 10^8 I$, RCAC drives the sampled error signal $z(k)$ to zero by converging to an internal model controller for the command frequencies $\Omega_1 = 0$ rad/sample and $\Omega_2 = 0.25$ rad/sample $= 1$ rad/sec. After convergence, the command-following error $\bar{z}(t)$ is small between consecutive sampling instants, as shown in Figure 2.

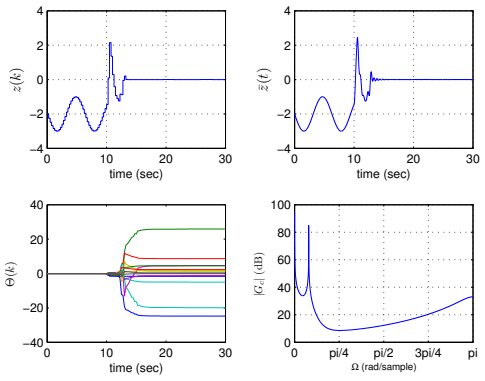

Fig. 2. Example 4.1: Undersampled disturbances. This figure illustrates the closed-loop response with no disturbances. Both the samples $z(k)$ and the actual continuous-time command-following error $\bar{z}(t)$ converge to zero, the controller gains converge, and RCAC converges to an internal model controller with high gain at the command frequencies 0 rad/sample and 0.25 rad/sample.

Now, we consider the same problem in the presence of the matched disturbance $\bar{w}(t) = 2.5 \sin 5\pi t$. Unlike $\omega_{{\rm N},r}$, the Nyquist rate $\omega_{{\rm N},w} = 10\pi$ rad/sec corresponding to $\bar{w}(t)$ is larger than the sampling rate $\omega_{\rm s} = 8\pi$ rad/sec and thus $\bar{z}(t)$ is undersampled at this sampling rate. Choosing the same control parameters, RCAC drives the sampled error signal $z(k)$ to zero by converging to an internal model controller for the command frequencies as well as the disturbance aliasing frequency $2\pi - 1.25\pi = 0.75\pi$ rad/sample. Thus the actual command-following error $\bar{z}(t)$ does not converge to zero due to aliasing, as shown in Figure 3.

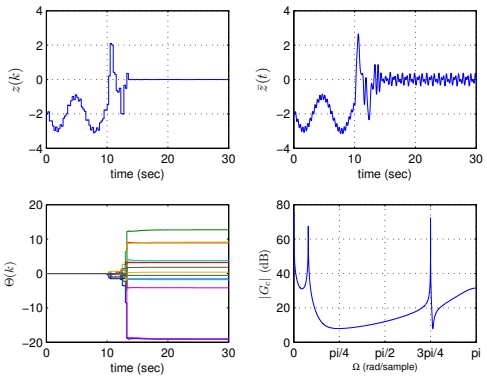

Fig. 3. Example 4.1: Undersampled disturbances. This figure illustrates the closed-loop response with the matched disturbance $\bar{w}(t) = 2.5 \sin 5\pi t$. The disturbance frequency is larger than the Nyquist frequency 4π rad/sample. RCAC drives the sampled performance $z(k)$ to zero, but the actual command-following error $\bar{z}(t)$ is nonzero between consecutive samples, due to disturbance aliasing. In addition to the command frequency, RCAC places an internal model into the disturbance aliasing frequency 0.75π rad/sample.

V. Numerical Examples with High-Frequency Dynamics

We now consider plants with lightly-damped, undamped, or unstable high-frequency dynamics, and, to investigate the performance of RCAC with aliasing of plant dynamics, we choose the sampling rate below the Nyquist rate corresponding to the free response of the plant. In each example, the controller $\Theta(k)$ is initialized to be zero, and cumulative RCAC is used with $\lambda = 1$ to update the controller.

Example 5.1: [Undersampled lightly-damped modes.] Consider the $4^{\rm th}$-order Lyapunov stable plant $T_{zu}(s) = 50\frac{(s+0.2+\jmath 3)(s+0.2-\jmath 3)}{(s+\jmath 1.5)(s-\jmath 1.5)(s+0.5+\jmath 10)(s+0.5-\jmath 10)}$. The goal is to have the output of the plant follow the command $\bar{r}(t) = \sin 0.5t$ while rendering the closed-loop system asymptotically stable. The plant is initialized with nonzero initial conditions so that the free response is nonzero.

First, we choose $\omega_{\rm s} = 4\pi$ rad/sec. Notice that the Nyquist frequency $\omega_{\rm s}/2$ is smaller than 10 rad/sec and thus the plant is undersampled due to the high-frequency component of the free response contributed by the lightly-damped modes. Choosing $n_{\rm c} = 6$, $P_0 = 10^5 I$ and $G_{\rm f}(\mathbf{q}^{-1}) = H_1\mathbf{q}^{-1}$, RCAC is turned on at $t = 5$ sec. RCAC drives the sampled command-following error $z(k)$ to zero, and the actual command-following error $\bar{z}(t)$ is small between consecutive sampling instants, as shown in Figure 4.

We now investigate the performance of RCAC when the lightly-damped modes of T_{zu} become uncontrollable due to

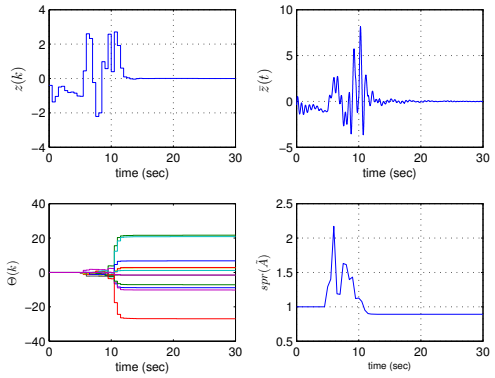

Fig. 4. Example 5.1: Undersampled asymptotically stable modes. This figure illustrates the closed-loop response with the command $\bar{r}(t) = \sin 0.5t$. The Nyquist frequency 2π rad/sec is smaller than the damped frequency 10 rad/sec corresponding to the lightly-damped modes. RCAC is turned on at $t = 5$ sec, drives both $z(k)$ and $\bar{z}(t)$ to zero, and stabilizes the closed-loop system.

sampling. For this, it follows from (6) that the sampling rate should be chosen so that $l\omega_{\mathrm{s}} = 20$ rad/sec, where l is a positive integer. We consider $l = 1$, that is, $\omega_{\mathrm{s}} = 20$ rad/sec, and thus $h = \pi/10$ sec/sample. This causes the sampled-data plant to have a stable pole-zero cancellation near -0.62. Choosing the same control parameters, RCAC is turned on at $t = 5$ sec. RCAC stabilizes the system and drives the sampled-command-following error to zero, and the command following error remains small between consecutive sampling instants. This examples suggests that undersampling of asymptotically stable dynamics does not harm the asymptotic performance of RCAC, even when these modes are uncontrollable due to sampling in accordance with Proposition 2.1.

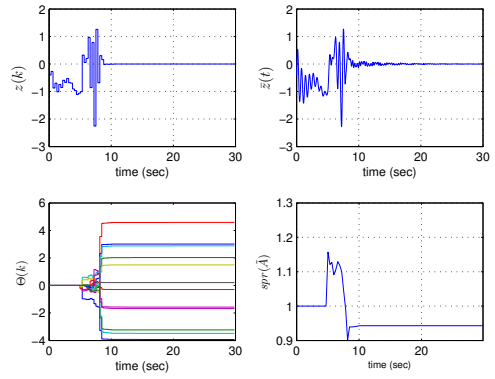

Fig. 5. Example 5.1: Undersampled asymptotically stable modes. This figure illustrates the closed-loop response with lightly-damped modes that are uncontrollable due to sampling. Nevertheless, RCAC drives both $z(k)$ and $\bar{z}(t)$ to zero, and the closed-loop sampled-data system is stable after convergence.

Example 5.2: [Undersampled undamped modes] Consider the 4^{th}-order Lyapunov stable plant $T_{zu}(s) = 50\frac{(s+0.2+\jmath 3)(s+0.2-\jmath 3)}{(s+\jmath 10)(s-\jmath 10)(s+0.5+\jmath 1.5)(s+0.5-\jmath 1.5)}$. The plant is initialized with the nonzero initial condition $x(0) = \begin{bmatrix} 0.0846 & -0.0229 & -0.0474 & -0.0083 \end{bmatrix}^{\mathrm{T}}$ in controllable canonical form. Due to the nonzero initial conditions, $\bar{z}(t)$ oscillates in open-loop, and the control objective is to drive $\bar{z}(t)$ to zero. Furthermore, at $t = 50$ sec, the matched sinusoidal disturbance $\bar{w}(t) = \mathbf{1}(t-50)25\sin(t)$ starts exciting the system. Therefore, the objective is to first regulate the output $\bar{z}(t)$ and then reject the disturbance $\bar{w}(t)$ from $\bar{z}(t)$. Note that the disturbance frequency is $\omega = 1$ rad/sec $= 0.16$ Hz.

We first sample the plant with $\omega_{\mathrm{s}} = 20\pi$ rad/sec $= 10$ Hz, which is faster than the Nyquist rate 20 rad/sec associated with the undamped modes. RCAC is turned on at $t = 20$ sec, and choosing $n_{\mathrm{c}} = 6$, $P_0 = 10^4 I$ and $G_{\mathrm{f}}(\mathbf{q}^{-1}) = H_1\mathbf{q}^{-1} = 0.23\mathbf{q}^{-1}$, both $z(k)$ and $\bar{z}(t)$ are driven to zero, and the closed-loop sampled-data system is asymptotically stable after convergence, as shown in Figure 6. Note that the controller readapts at $t = 50$ sec in order to reject the disturbance $\bar{w}(t)$.

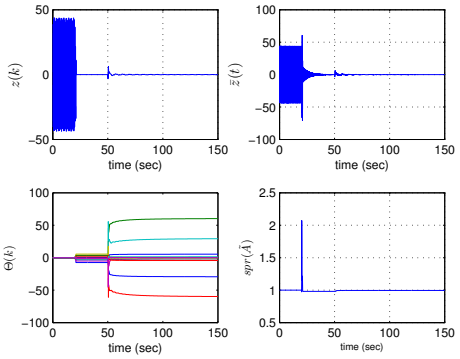

Fig. 6. Example 5.2: Undersampled undamped modes. This figure illustrates the closed-loop response with sufficiently fast sampling, that is, the sampling rate 20π rad/sec is faster than the Nyquist rate corresponding to the disturbance and the dynamics. RCAC first stabilizes the system and then readapts at $t = 50$ sec to reject the disturbance. The spectral radius of the closed-loop system is 0.99 after convergence.

Now, we sample the plant with $\omega_{\mathrm{s}} = 20$ rad/sample $= 10/\pi$ Hz. The sampled-data plant is uncontrollable at this sampling rate, and the uncontrollable modes correspond to the undamped modes of the continuous-time plant. Choosing $n_{\mathrm{c}} = 6$, $P_0 = 10^4 I$, and $G_{\mathrm{f}}(\mathbf{q}^{-1}) = H_1\mathbf{q}^{-1} = \mathbf{q}^{-1}$, the closed-loop response is shown in Figure 7. The first observation is the inability of the adaptive controller to reduce the spectral radius of the closed-loop sampled-data system below 1. This is expected, because the undamped modes are uncontrollable due to sampling. The second observation is that, despite the fact that $z(k)$ converges to zero, the intersample values of $\bar{z}(t)$ are large, in fact, in steady-state, $\bar{z}(t)$ has a peak magnitude of about 22. To study the cause of large intersample behavior, we make a spectral analysis of $\bar{z}(t)$ after convergence. Figure 8 shows the power spectral density of $\bar{z}(t)$ for $t > 100$. In particular, we notice spikes near frequencies $\omega_1 = 0.16$ Hz, $\omega_2 = 1.59$ Hz, $\omega_3 = 3.04$ Hz and $\omega_4 = 3.34$ Hz. Note that ω_1 is exactly the frequency ω of the disturbance signal $\bar{w}(t)$. Furthermore, $\omega_3 = \omega_{\mathrm{s}} - \omega_1$, and $\omega_4 = \omega_{\mathrm{s}} + \omega_1$ are alias frequencies associated with the disturbance frequency ω and sampling rate ω_{s}. However, the spike with the largest magnitude corresponds to ω_2, which is exactly the frequency of the undamped modes. Note that ω_2 is also the Nyquist frequency of the sampled-data system. The large intersample oscillations in $\bar{z}(t)$ are therefore caused by the aliasing effects associated with the undamped, uncontrollable modes of the continuous-time plant.

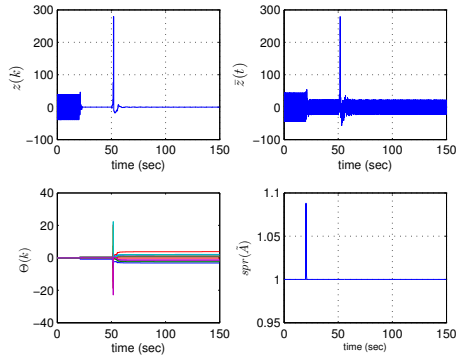

Fig. 7. Example 5.2: Undersampled undamped modes. This figure illustrates the closed-loop response with undamped modes that are uncontrollable due to sampling. Although RCAC drives the sampled output $z(k)$ to zero, the actual continuous-time signal $\bar{z}(t)$ is not equal to zero between sampling instants. Since the undamped modes are uncontrollable, RCAC cannot decrease the closed-loop spectral radius below 1.

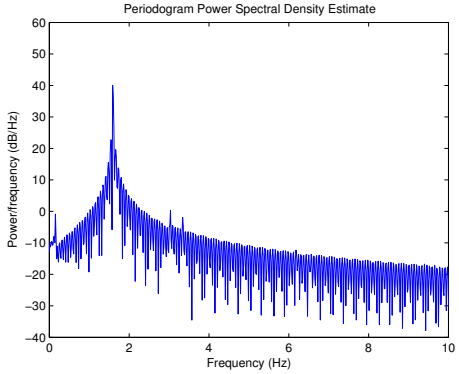

Fig. 8. Example 5.2: Undersampled undamped modes. This figure illustrates the power spectral density of the closed-loop performance $\bar{z}(t)$ shown in Figure 7 in steady-state. The largest peak in the spectral content is near 1.59 Hz, which is the frequency of the uncontrollable, undamped modes.

Finally, we reconsider the same problem with $\omega_{\mathrm{s}} = 4\pi$ rad/sample $= 2$ Hz, which is slower than the Nyquist rate corresponding to the undamped modes. The continuous-time plant is thus undersampled, however, the sampled-data plant does not lose controllability due to sampling. Furthermore, the sampled-data plant now has a NMP sampling zero near -1.34. Choosing $n_{\mathrm{c}} = 6$, $P_0 = 10^4 I$, and $G_{\mathrm{f}}(\mathbf{q}) = H_1 \frac{(\mathbf{q}+1.34)}{\mathbf{q}^2}$, the closed-loop response is shown in Figure 9. We observe that before the disturbance is introduced, both $z(k)$ and $\bar{z}(t)$ are driven to zero, and then, after the disturbance is introduced, $z(k)$ converges to zero after a transient period, although $\bar{z}(t)$ exhibits intersample oscillations. This suggests that the intersample oscillations are caused by the aliasing effects associated with the disturbance, rather than the undamped modes. The power spectral density of $\bar{z}(t)$ shown in Figure 10 confirms this view, as the spikes in the spectral density are near ω, and the alias frequencies $l\omega_{\mathrm{s}} \pm \omega$, where l is a positive integer. In conclusion, aliasing of the undamped dynamics causes trouble only if these modes are uncontrollable due to sampling. Otherwise, RCAC moves these modes inside the unit circle so that the natural response of the closed-loop plant converges to zero as t increases.

Example 5.3: [Undersampled unstable modes]

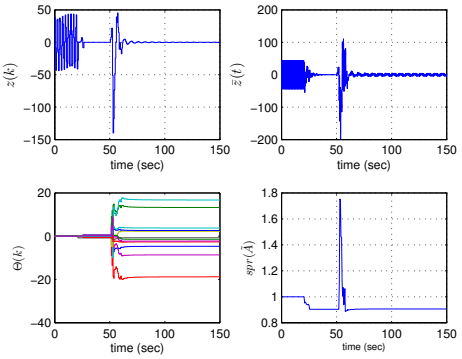

Fig. 9. Example 5.2: Undersampled undamped modes. Sampling rate 4π rad/sec is now lower than the Nyquist rate corresponding to the undamped modes, however, these modes are now controllable after sampling. The output first oscillates due to nonzero initial conditions, and then, RCAC is turned on at $t = 20$ sec, and drives both $z(k)$ and $\bar{z}(t)$ to zero. Then, at $t = 50$ sec, the disturbance starts exciting the system, RCAC readapts, and rejects the disturbance from $z(k)$. However, $\bar{z}(t)$ is nonzero between sampling instants due to disturbance aliasing.

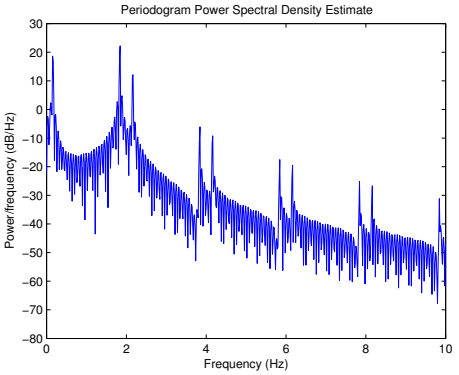

Fig. 10. Example 5.2: Undersampled undamped modes. This figure illustrates the power spectral density of the closed-loop performance $\bar{z}(t)$ shown in Figure 7 in steady-state. The power spectral density does not have a peak near the frequency of the undamped modes. Rather, the peaks are near the disturbance frequency ω and aliased frequencies $l\omega_{\mathrm{s}} \pm \omega$, where l is a positive integer.

Consider the 4^{th}-order unstable plant $T_{zu}(s) = 20\frac{(s+0.6)(s+1.5)}{(s-1+\jmath 10)(s-1-\jmath 10)(s+0.5+\jmath 1.5)(s+0.5-\jmath 1.5)}$. The plant is initialized with the nonzero initial conditions $x(0) = \begin{bmatrix} -0.09 & 0.03 & -0.02 & -0.005 \end{bmatrix}^{\mathrm{T}}$ in controllable canonical form. The control objective is to stabilize the closed-loop system and drive the output $\bar{z}(t)$ to zero.

It follows from (6) that if the sampling rate is chosen to be $\omega_{\mathrm{s}} = 20/l$, where l is a positive integer, sampled-data control of T_{zu} becomes impractical, since the unstable modes are uncontrollable due to sampling.

Now, to investigate the effects of undersampling of unstable (but controllable) modes, we sample $T_{zu}(s)$ with $\omega_{\mathrm{s}} = 2\pi$ rad/sample $= 1$ Hz. Note that ω_{s} is slower than the Nyquist rate 20 rad/sample corresponding to the unstable modes. Furthermore, the sampled-data system has a NMP sampling zero near -2.91. RCAC is turned on at $t = 2$ sec with $n_{\mathrm{c}} = 4$, $P_0 = 1000I$, and $G_{\mathrm{f}}(\mathbf{q}) = H_1 \frac{(\mathbf{q}+2.91)}{\mathbf{q}^2}$. Since the sampling rate is chosen to be slow, the output $\bar{z}(t)$ undergoes large transients, but nevertheless, RCAC stabilizes the plant, and both $z(k)$ and $\bar{z}(t)$ converge to zero in about

30 seconds, which is 30 time steps, as shown in 11.

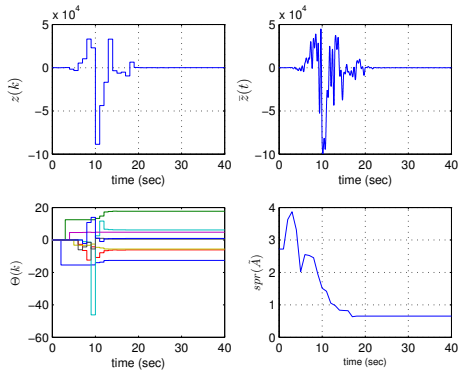

Fig. 11. Example 5.3: Undersampled unstable modes. This figure illustrates the closed-loop response with the sampling rate 2π rad/sample, which is slower than the Nyquist rate 20 rad/sample corresponding to the unstable modes. The plant is initialized with nonzero initial conditions, and therefore, the output $\bar{z}(t)$ first diverging away from zero. Then, at $t = 2$, RCAC is turned on. Since the sampling rate and therefore the sampled-data controller is slow, the output $\bar{z}(t)$ undergoes large transients before controller convergence, but eventually, RCAC stabilizes the plant, and drives both $z(k)$ and $\bar{z}(t)$ to zero.

Indeed, transient performance and convergence time can be improved by sampling faster. For example, choosing $\omega_{\mathrm{s}} = 20\pi$ rad/sample $= 10$ Hz, $n_{\mathrm{c}} = 4$, $P_0 = 1000I$, and $G_{\mathrm{f}}(\mathbf{q}) = H_1 \frac{\mathbf{q}^{-1}+1.1}{\mathbf{q}^2}$, RCAC is turned on at $t = 2$ sec. Now, $\bar{z}(t)$ converges to zero in about 30 time steps, which is the same as in the previous case, but since a time step is equal to 0.1 sec, convergence occurs in only 3 sec, and the transient performance is much better compared to Figure 11 as shown in Figure 12.

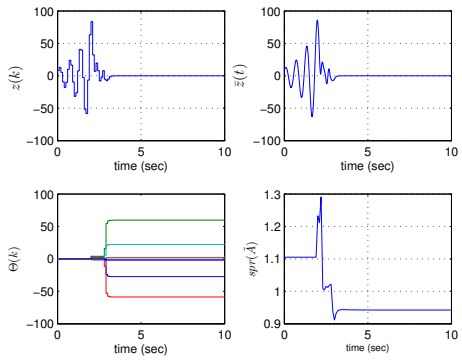

Fig. 12. Example 5.3: Undersampling of unstable modes. This figure illustrates the closed-loop response with the sampling rate 20π rad/sample, which is ten times faster than the sampling rate of Figure 11. The convergence is faster, and the transient performance is better compared to Figure 11.

In conclusion, the adaptive controller is able to stabilize the unstable plant even if the unstable modes are undersampled, however, if the sampling rate and therefore the controller is too slow, the output may become too large before it can be regulated by the controller, and therefore, undersampling the unstable modes may be undesirable in practice. Obviously, the sampling rate should be chosen so that the unstable modes of the system are controllable.

VI. CONCLUSIONS

We presented a numerical investigation of retrospective cost adaptive control (RCAC) applied to sampled-data control in the presence of aliasing of dynamics and disturbances. It is shown that RCAC stabilizes plant even if the high-frequency unstable modes are undersampled. However, even if the samples of the performance variable converge to zero, intersample command following error may be nonzero due to aliasing of disturbances. If the disturbance frequency is larger than the Nyquist frequency, RCAC converges to an internal model controller with high gain at the aliased disturbance frequency. Controllability loss due to sampling is also considered, and it is shown that the performance of RCAC is not degraded as long as the uncontrollable modes are stable.

REFERENCES

[1] S. L. Osburn and D. S. Bernstein, "An Exact Treatment of the Achievable Closed-Loop H_2 Performance of Sampled-data Controllers: from Continuous-time to Open-loop," *Automatica*, Vol. 31, No. 4, pp. 617–620, 1995.

[2] R. E. Kalman, Y. C. Ho, and K. S. Narendra, "Controllability of Linear Systems," *Contributions to Differential Equations*, Vol. 1, No. 2, pp. 189–213, Interscience, New York.

[3] T. Chen and B. A. Francis, *Optimal Sampled-Data Control Systems*, Springer, 1996.

[4] C. E. Rohrs, L. Valavani, M. Athans, and G. Stein, "Robustness of Continuous-Time Adaptive Control Algorithms in the Presence of Unmodeled Dynamics," *IEEE Trans. Autom. Contr.,* Vol. 30, No. 9, pp. 881–889, Sep 1985.

[5] E. D. Sumer and D. S. Bernstein, "Robust Sampled-Data Adaptive Control of Rohrs Counterexamples," *Proc. Conf. Dec. Contr.,* Maui, HI, December 2012.

[6] A. Feuer and G. C. Goodwin, "Generalized Sample Hold Functions–Frequency Domain Analysis of Robustness, Sensitivity, and Intersample Difficulties," *IEEE Trans. Autom. Contr.,* Vol. 39, No. 5, May 1994.

[7] M. J. Blachuta, "Continuous-time Design of Discrete-time Control Systems," *Proc. 1997 Europ. Contr. Conf.,* Brussels, Belgium, 1997.

[8] G. Langholz and Y. Bar-Ness, "On Observability of Sampled-Data Systems," *Int. J. Systems Sci.,* Vol. 8, No. 6, pp. 697–704, 1977.

[9] M. A. Santillo and D. S. Bernstein, "Adaptive Control Based on Retrospective Cost Optimization", *AIAA J. Guid. Contr. Dyn.*, Vol. 33, pp. 289–304, 2010.

[10] J. B. Hoagg and D. S. Bernstein, "Retrospective Cost Model Reference Adaptive Control for Nonminimum-Phase Systems," *AIAA J. of Guid. Contr. Dyn.,* Vol. 35, No. 6, pp. 1767–1786, 2012.

[11] A. M. D'Amato, E. D. Sumer, and D. S. Bernstein, "Frequency-Domain Stability Analysis of Retrospective Cost Adaptive Control for Systems with Unknown Nonminimum-Phase Zeros," *Proc. Conf. Dec. Contr.*, Orlando, FL, December 2011.

[12] E. D. Sumer, A. M. D'Amato and D. S. Bernstein, "Robustness of Retrospective-Cost Adaptive Control to Markov-Parameter Uncertainty," *Proc. Conf. Dec. Contr.*, pp. 6085–6090, Orlando, FL, December 2011.

[13] E. D. Sumer and D. S. Bernstein, "Retrospective Cost Adaptive Control with Error-Dependent Regularization for MIMO Systems with Uncertain Nonminimum-Phase Transmission Zeros," AIAA Guid. Nav. Contr. Conf., Minneapolis, MN, August 2012, AIAA-2012-4670-123.